Heuristic optimization of analytic laser pulses for vibrational stabilization of ultracold KRb

Article *in* The Journal of Chemical Physics · December 2018

DOI: 10.1063/1.5052019

3 authors:

Ruben Guerrero
Stanford University
15 PUBLICATIONS **40** CITATIONS
SEE PROFILE

Maria Alejandra Castellanos
Massachusetts Institute of Technology
9 PUBLICATIONS **119** CITATIONS
SEE PROFILE

Carlos Alberto Arango
ICESI University
34 PUBLICATIONS **308** CITATIONS
SEE PROFILE

Heuristic optimization of analytic laser pulses for vibrational stabilization of ultracold KRb

Cite as: J. Chem. Phys. **149**, 244110 (2018); https://doi.org/10.1063/1.5052019
Submitted: 13 August 2018 . Accepted: 04 December 2018 . Published Online: 27 December 2018

Rubén D. Guerrero, Maria A. Castellanos, and Carlos A. Arango

Heuristic optimization of analytic laser pulses for vibrational stabilization of ultracold KRb

Rubén D. Guerrero,[1,a)] Maria A. Castellanos,[2,3,b)] and Carlos A. Arango[2,c)]
[1]*PULSE Institute and Department of Chemistry, Stanford University, Stanford, California 94305, USA*
[2]*Department of Chemical Sciences, Universidad Icesi, Cali, Colombia*
[3]*Department of Chemistry, Massachusetts Institute of Technology, Cambridge, Massachusetts 02139-4307, USA*

(Received 13 August 2018; accepted 4 December 2018; published online 27 December 2018)

We proposed a methodology that allows to maximize the population transfer from a high vibrational state of the $a^3\Sigma^+$ triplet state to the vibrational ground state of the $X^1\Sigma^+$ singlet state though the optimization of one pump and one dump laser pulses. The pump pulse is optimized using a fitness function, heuristically improved, that includes the effect of the spin-orbit coupling of the KRb [b-A]-scheme. The dump pulse is optimized to maximize the population transfer to the ground state. We performed a comparison with the case in which the pump and dump pulses are optimized to maximize the population transfer to the ground state employing a genetic algorithm with a single fitness function. The heuristic approach turned out to be 70% more efficient than a quantum optimal control optimization employing a single fitness function. The method proposed provides simple pulses that have an experimental realm. *Published by AIP Publishing.* https://doi.org/10.1063/1.5052019

I. INTRODUCTION

Ultracold polar molecules are of central interest in emergent research fields as quantum phase transitions,[1,2] ultracold chemistry,[3–5] strongly correlated quantum systems,[2] and new schemes for quantum information processing.[6] In contrast with ultracold atoms, ultracold polar molecules offer the possibility to study the effect of anisotropic long-range interactions in the collective quantum dynamics of strongly correlated many body systems.[7,8] Cold and ultracold controlled chemistry are possible only when the translational energy of the colliding atoms is less than the perturbation of external fields, because thermal motion randomizes molecular collisions and precludes the coherent control by the external fields.[9] Applications of ultracold controlled chemistry are reported in a wide range of studies, from the role of scattering resonances in chemical reactions[10] to the importance of intermolecular forces in the determination of chemical reactivity.[11]

There are several experimental strategies to obtain cold molecules. Some methods attempt direct cooling over molecules, such as Stark[12,13] or Zeeman[14,15] decelerators, or buffer gas cooling.[16] However, laser cooling from cold molecules is experimentally challenging because of the internal complexity of molecules.[17] Other methods to obtain cold molecules use dense samples of cold atoms, which are used to create cold molecules by magnetic tuning of Feshbach resonances[8,18,19] or by photoassociation.[20–24] The resulting cold molecules stay in high vibrational levels, close to the dissociation limit, and additional steps are necessary to steer the molecule toward the ground vibrational level.[25] Stimulated rapid adiabatic passage (STIRAP)[26,27] has been successfully employed for producing ultracold molecules from weakly bound Feshbach resonance molecular states.[8,18,28,29] Although STIRAP has been experimentally successful in obtaining ultracold diatomic molecules,[8,29] it requires the previous identification of an intermediate state connecting the initial state with the ground vibrational and electronic state of the molecule.[19,29] However, advances in the fields of laser stabilization and generation of femtosecond laser combs[30] would allow STIRAP to work arbitrary energy gaps,[8,29,31] even though STIRAP requires the ability to maintain the phase coherence between Raman lasers of different frequency.[26]

Promising schemes have been proposed for producing ground vibrational molecules by considering the use of shaped laser pulses.[22–24,31] The first theoretical scheme proposed to obtain $v = 0$ molecules was based on the use of linear chirped pulses (LCP) to pump the initial wave packet to an excited energy curve. This scheme was applied to Cs_2 achieving improvement of the efficiency of obtaining cold molecules compared with proposals based on CW laser pulses only.[32,33] The use of genetic algorithms for the pump pulse optimization has been proposed theoretically to obtain ultracold Rb_2 molecules at a specific ground state level; this approach showed considerable enhancement of the cold molecules yield compared with the use of unshaped pulses.[34] In recent work, nanosecond shaped pulses have been proposed to enhance the production of ultracold Rb_2 molecules.[35] Researchers have demonstrated experimentally and theoretically the advantages of using shaped pulses not only for pumping the initial wave packet to the excited states but also on dumping it to the ground electronic state by stimulated emission.[35–38]

Gradient-based optimal control theory has been widely employed in chemical physics.[39–41] Quantum Optimal Control (QOC) based on Krotov's algorithm has been used to obtain ultracold Na_2 and KRb molecules from weakly bound

[a)]Electronic mail: rguerrer@stanford.edu
[b)]Electronic mail: mariacm@mit.edu
[c)]Electronic mail: caarango@icesi.edu.co

excited molecules.[25,42] Ndong and Koch[25] showed the possibility of obtaining ground vibrational KRb molecules from Feshbach molecules by employing shaped lasers. Although Feshbach molecules are always produced in a linear superposition of triplet $a^3\Sigma^+$ and singlet $X^1\Sigma^+$ states, the present work focuses on the study of the transfer of KRb molecules from an initial vibrational state of the $a^3\Sigma^+$ triplet to the ground vibrational state of the $X^1\Sigma^+$. This vibrational stabilization is carried out by employing a pseudospectral formulation of the QOC based on genetic algorithms (QOC+GA).[43] In future works, we will apply the proposed QOC+GA methodology on realistic Feshbach molecules.

The importance of spin-orbit coupling (SOC) in the formation of ultracold molecules has been assessed and employed for Rb_2, RbCs, and KRb.[22,23,25] In this work, we propose a heuristic approach to find an effective fitness function aimed to ease and make more efficient the pulse optimization. The result of our approach is an effective fitness function that accounts for both the pump and dump processes and also the spin-orbit coupling between the electronic curves $b^3\Pi$ and $A^1\Sigma$.

This paper is organized as follows: In Sec. II, we define the KRb nuclear and electronic system and describe the generalities of our QOC+GA method. Section III is divided into three subsections. The first subsection (Sec. III A) discusses the time scales associated with the dynamical evolution of the system. The second subsection (Sec. III B) displays the results of a traditional QOC approach in which a single fitness function is employed to reach the target state. The third subsection (Sec. III C) describes the results of a proposed approach where a heuristic improvement is performed to obtain an effective fitness function that accounts for the pump and spin-orbit coupling. A comparison between the effectiveness of both approaches is found throughout this section. Finally, conclusions are presented in the final section of this paper.

II. THEORETICAL MODEL AND METHODS

We are considering the set of potential energy curves (PECs), transition dipole moments (TDMs), and spin-orbit coupling (SOC) corresponding to the [*b*-*A*]-scheme of $^{39}K^{87}Rb$ molecule,[19] presented in Fig. 1. This [*b*-*A*]-scheme includes two singlet states: $X^1\Sigma^+$ and $A^1\Sigma^+$ and two triplet states: $a^3\Sigma^+$ and $b^3\Pi$. The corresponding Born–Oppenheimer PECs are V_X, V_A, V_a, and V_b respectively. Two TDMs are considered in the [*b*-*A*]-scheme: one TDM coupling the PECs belonging to the singlet manifold $\hat{d}_{XA}$ and the other TDM coupling the PECs within the triplet manifold $\hat{d}_{ab}$. At the same time, we included a SOC between triplet and singlet excited states, which consists of a diagonal element, $\hat{W}_{bb}$, and a nondiagonal element, $\hat{W}_{bA}$.

In atomic units, kinetic and potential energy operators of the Hamiltonian, $\hat{\mathcal{H}} = \hat{\mathcal{T}} + \hat{\mathcal{V}}$, are: $\hat{\mathcal{T}} = (-1/2m)\partial^2/\partial R^2$, and

$$\hat{\mathcal{V}} = \begin{pmatrix} \hat{V}_X(R) + \varepsilon_D(t)\hat{D}_X(R) & 0 & 0 & \varepsilon_D(t)\hat{d}_{XA}(R) \\ 0 & \hat{V}_a(R) + \varepsilon_P(t)\hat{D}_a(R) & \varepsilon_P(t)\hat{d}_{ba}(R) & 0 \\ 0 & \varepsilon_P(t)\hat{d}^\dagger_{ba}(R) & \hat{V}_b(R) + \hat{W}^\dagger_{bb}(R) & \hat{W}^\dagger_{bA}(R) \\ \varepsilon_D(t)\hat{d}^\dagger_{XA}(R) & 0 & \hat{W}^\dagger_{bA}(R) & \hat{V}_A(R) \end{pmatrix}. \quad (1)$$

We have included the permanent dipole moments $\hat{D}_X$ and $\hat{D}_a$ used in a previous work,[44] in order to incorporate pure vibrational transition induced by the coupling with the laser pulses.

The proposed control scheme employs two linear chirp pulses (LCPs). A first pulse, the pump pulse $\varepsilon_P(t)$, triggers the excitation of the KRb from the first electronic triplet state, $a^3\Sigma^+$, to the second triplet state, $b^3\Pi$. Shortly after, a dump pulse $\varepsilon_D(t)$ stimulates the transition between the excited and ground electronic singlet states, $A^1\Sigma^+$ and $X^1\Sigma^+$, respectively. In order to ensure independence between pump and dump mechanisms, the triplet–triplet and singlet-singlet transitions are affected only by their corresponding resonant pulse, accounting for the orthogonality of the two spin manifolds.

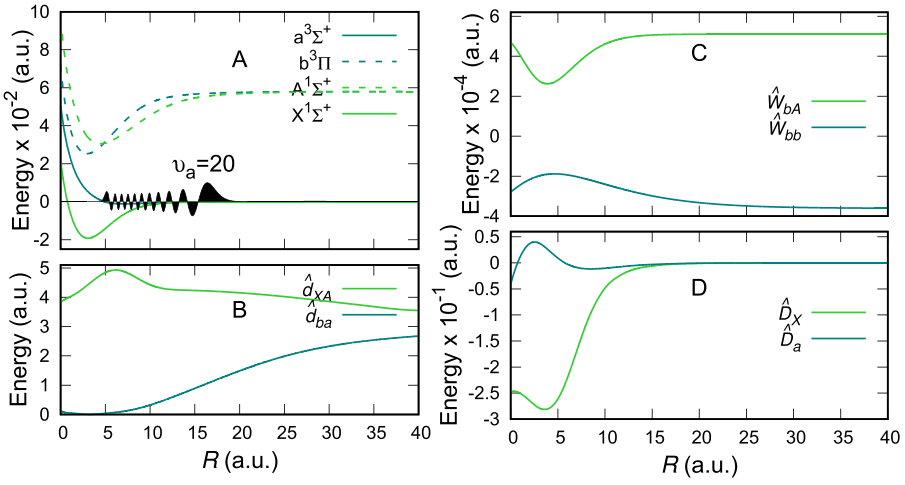

FIG. 1. The [*b*-*A*]-scheme for the $^{39}K^{87}Rb$ diatomic molecule.[19] (a) Potential energy curves (PECs). (b) Transition dipole moments (TDMs) for the $\{a^3\Sigma^+, b^3\Pi\}$ ($\hat{d}_{ab}$) and the $\{A^1\Sigma^+, X^1\Sigma^+\}$ ($\hat{d}_{XA}$) interactions.[19] (c) Spin-orbit (SO) diagonal ($\hat{W}_{bb}$) and off-diagonal ($\hat{W}_{bA}$) couplings.[19] (d) Permanent dipole moments (PDMs) of the $a^3\Sigma^+$ ($\hat{D}_a$) and $X^1\Sigma^+$ ($\hat{D}_X$) electronic states.[44]

Experimentally, this can be achieved by the use of polarized laser pulses, where the singlet transition is mediated by linearly polarized light and the triplet transitions by circularly polarized light.[25]

Each of the pump and dump pulses, $\varepsilon(t)$, are proposed as Gaussian LCPs with time profile[43,45]

$$\varepsilon(t) = E_0 \exp\left[-\frac{(t-\tau_0)^2}{2\tau^2}\right] \cos\left[\omega_0(t-\tau_0) + \tfrac{1}{2}c(t-\tau_0)^2\right], \tag{2}$$

where τ_0 the time shift, E_0 the pulse amplitude, ω_0 the central frequency, c the chirp constant, and τ the pulse width.

The state of the molecule as a function of time is

$$\Psi(R,t) = \psi_X(R,t)\chi_X + \psi_a(R,t)\chi_a + \psi_b(R,t)\chi_b + \psi_A(R,t)\chi_A, \tag{3}$$

with χ_α as the orthonormal electronic states and $\psi_\alpha(R, t)$ as the nuclear wave function on curve α.

The nuclear wave functions in (3) are obtained by solving the time-dependent Schrödinger equation (TDSE),

$$\frac{\partial\Psi(R,t)}{\partial t} = -i\hat{\mathcal{H}}(t)\Psi(R,t). \tag{4}$$

As a result of the interaction with the pulse shape, the formal solution of the TDSE, (4), is the Green's function or short-time propagator, $\hat{U}(t,0) = e^{-i\int_0^{\delta t}[\hat{\mathcal{H}}(t')]dt'}$. Numerically, we calculate an approximation to the short-time propagator by employing the midpoint rule to approximate the time integration, $\hat{U}(t+\delta t,t) = e^{-i\int_t^{t+\delta t}[\hat{\mathcal{H}}(t')]dt'} \approx e^{-i\mathcal{H}(t+\delta t/2)\delta t}$; the validity of this approximation is conditioned to $\hbar\omega\delta t \ll 1$, with $\hbar\omega$ standing for the minimum energy of any process taking place in the simulation. The error associated to employing a midpoint rule is $\mathcal{O}(\delta t^3)$. The short-time propagator can be further approximated using the symmetric Strang splitting as follows:[43,46]

$$e^{-i\hat{\mathcal{H}}2\delta t} \approx e^{-i\hat{\mathcal{T}}\delta t}e^{-i\hat{\mathcal{V}}2\delta t}e^{-i\hat{\mathcal{T}}\delta t}. \tag{5}$$

QOC+GA method will be used to obtain KRb molecules in the ground vibrational state of the ground electronic state $X^1\Sigma^+$, starting from an excited Feshbach resonant state. We will consider a vibrational stabilization mechanism starting from three different excited vibrational states of the $a^3\Sigma^+$ PEC: $\varphi_{a,29}$, $\varphi_{a,24}$, and $\varphi_{a,20}$. A stabilization scheme starting from $\varphi_{a,29}$ has been previously studied using a STIRAP methodology,[19] while $\varphi_{a,24}$ was used as the initial state in a Krotov self-consistent procedure.[25] It is important to remark that the experimental realm of the resulting optimal pulse shapes obtained using gradient-based methodology is a concern in this work. It is shown that in our control scheme, the $\varphi_{a,20}$ initial state is considerably more efficient in producing ground state molecules than the $\varphi_{a,24}$ and $\varphi_{a,29}$. The $\varphi_{a,29}$ and $\varphi_{a,24}$ vibrational states correspond to weakly bound KRb molecules obtained by ramping a magnetic field over a Feshbach resonance,[24] while the $\varphi_{a,20}$ initial state is just slightly lower in vibrational energy. The vibrational eigenvectors, $\varphi_{\alpha,\upsilon}(R)$, for each of the three initial states considered here are obtained by employing Colbert–Miller discrete variable representation (DVR) method.[47] A grid of 55 a.u. and 2200 grid points was used for the propagation starting from initial states $\varphi_{a,20}$ and $\varphi_{a,24}$, meanwhile a grid of 79.975 a.u and 3200 grid points was used for the propagation starting from initial state $\varphi_{a,29}$.

An educated initial guess for a favorable transferring mechanism can be found by considering the transition matrix elements (TMEs), between the vibrational levels of the electronic states:

$$\mu_{\alpha,\beta}^{\upsilon_\alpha,\upsilon_\beta} = \left\langle \varphi_{\alpha,\upsilon_\alpha}\middle|\hat{\mu}_{\alpha,\beta}\middle|\varphi_{\beta,\upsilon_\beta}\right\rangle. \tag{6}$$

In (6), integration is carried out over the entire domain of the R variable. In this equation, the paired indices α, β correspond to the coupled states $a^3\Sigma^+$ and $b^3\Pi$ [Fig. 2(a)], $b^3\Pi$ and $A^1\Sigma^+$ [Fig. 2(b)], and $A^1\Sigma^+$ and $X^1\Sigma^+$ [Fig. 2(c)]. The indices υ_α and υ_β denote specific vibrational levels in the electronic states α and β, respectively. The operator $\hat{\mu}_{\alpha,\beta}$ is the coupling between the electronic states α and β, these being $\hat{d}_{ab}$ for the coupling $\mu_{a,b}^{\upsilon_a,\upsilon_b}$, the spin-orbit coupling $\hat{W}_{bA}$ for $\mu_{b,A}^{\upsilon_b,\upsilon_A}$, and $\hat{d}_{XA}$ for coupling $\mu_{A,X}^{\upsilon_A,\upsilon_X}$. The calculated TMEs are shown in Fig. 2.

A simple analysis based only on the TMEs allows to find an optimal stabilization pathway connecting the absolute ground state with the vibrational states of $a^3\Sigma^+$. As indicated by the red circle in Fig. 2(c), $\varphi_{X,0}$ only couples with low vibrational levels in $A^1\Sigma^+$, around $\upsilon_A \approx 11$. Although the red circle in 2(b) shows that the $\upsilon_A \approx 11$ levels display significant coupling with $\upsilon_b < 35$, the $\upsilon_b < 35$ levels have no significant coupling with vibrational levels of $a^3\Sigma^+$, except for a small coupling with levels $\upsilon_a \approx 3$ [red circle in Fig. 2(a)]. Thus, a

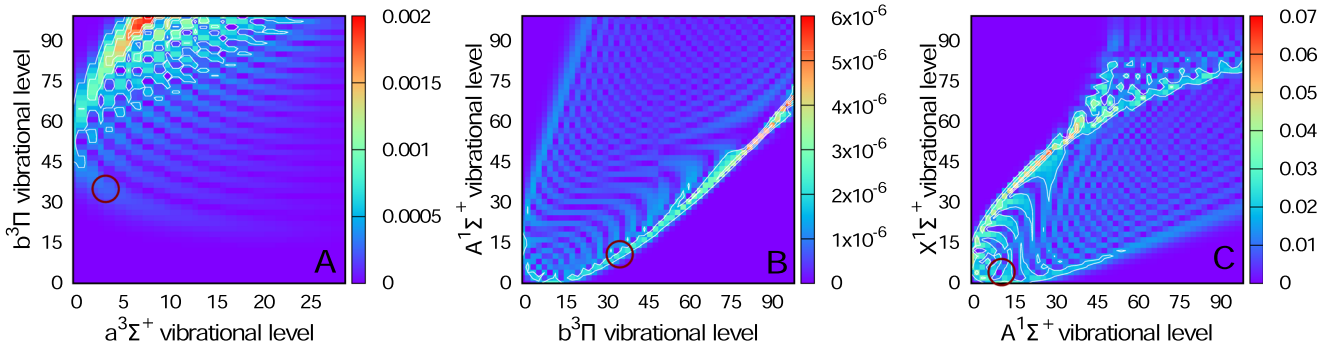

FIG. 2. TMEs between vibrational levels of KRb potential energy curves (PECs).[19] (a) TMEs between the triplet states $a^3\Sigma^+$ and $b^3\Pi$, (b) the spin-orbit coupling TMEs between $b^3\Pi$ and $A^1\Sigma^+$ states, and (c) the TMEs between singlet states: $A^1\Sigma^+$ and $X^1\Sigma^+$. Red circles in each of the panels mark the vibrational states composing the optimal path for vibrational stabilization down to $\varphi_{X,0}$ ground state.

vibrational stabilization scheme based on purely TME transitions from initial excited states of $a^3\Sigma^+$ will mostly end up in vibrationally excited $X^1\Sigma^+$ molecules.[25]

We propose two different approaches to reach the absolute ground state $\varphi_{X,0}$. In the first approach (direct mechanism), we directly targeted the ground state $\varphi_{X,0}$ by designing the appropriate fitness function for our QOC+GA methodology. In the second approach (assisted mechanism), we assumed a vertical transition of the vibrational state $\varphi_{X,0}$ from $X^1\Sigma^+$ to $A^1\Sigma^+$. Once the state $\varphi_{X,0}$ is located on $A^1\Sigma^+$, we allowed it to evolve on curves $A^1\Sigma^+$ and $b^3\Pi$ including the SOC, under the reduced Hamiltonian

$$\hat{\mathcal{H}} = \begin{pmatrix} \hat{T} + \hat{V}_b(R) + \hat{W}^{\dagger}_{bb}(R) & \hat{W}^{\dagger}_{bA}(R) \\ \hat{W}^{\dagger}_{bA}(R) & \hat{T} + \hat{V}_A(R) \end{pmatrix}. \tag{7}$$

The vibrational decomposition of the wave packet $\varphi_{X,0}$ on $A^1\Sigma^+$ and $b^3\Pi$ allowed us to find optimal pulses exploiting the action of the SOC on the wave packet. Further details about the aforementioned approaches can be found in Sec. III.

Our aim in this contribution is to apply the QOC+GA methodology,[43] in order to find an optimal sequence of LCPs capable of producing KRb molecules on the $X^1\Sigma^+$ singlet in a vibrational state as low as possible constrained to have experimental realm. A further advantage of our method is that once the pulse is optimized, the dynamics induced by the pulse is computationally reproducible by any other correct software, and the resulting optimal pulse shape is transferable between the researchers for future use either as starting point for further optimization on the same Hamiltonian or for simulating the physical process induced by the pulse *per se*. Features of paramount importance for bringing systematization to the control of quantum processes in analogy to the systematization of electronic structure due to the introduction Gaussian basis sets. Even further, the constraint to parameters that are experimentally feasible is a step toward turning the optimal control simulations into useful technology.

In order to achieve pulses within the experimental realm, we constraint the pulse shapes to LCPs as in (2), at the same time constraining the LCPs to a set of parameters that are within experimental reach, using state-of-the-art pulse-shaping technology. The QOC+GA methodology was previously employed for achieving active control of the dissociation of diatomic molecules[43] and for the photoisomerization of retinal.[46] In the present contribution, the chromosome of the i-th individual corresponds to the concatenation of the parameters of the LCP (2) of the pump, γ_P, and dump, γ_D, LCPs, or vectors of genes, $\Gamma_i = \{\gamma_P, \gamma_D\}$. Each LCP is represented by a 5 vector of parameters $\gamma_j = (E_0, \tau_0, c, \tau, \omega_0)$. As is standard in the QOC+GA methodology, we employed two genetic operations in order to evolve the initial population of individuals through the optimization cycle: (1) a mutation to change one or more genes (parameters) with probability π_M and (2) a crossover operation that combines two individuals to generate a new one with probability π_X. The chromosome of the new individual (child) is generated as a fitness-weighted combination of the chromosomes of the parents. For the direct mechanism, we employed the genes $\gamma_{P,D} = (E_0, \tau_0, c = 0, \tau, \omega_0)$ for the pump and dump pulses, i.e., Gaussian pulses. In the assisted mechanism, we employed the QOC+GA separately for the pump and dump pulses with genes $\gamma_{P,D} = (E_0, \tau_0, c, \tau, \omega_0)$, i.e., LCPs.

In order to set up the optimization of the pulses via genetic algorithms, we need an initial set of individuals (the first generation) and a fitness function to score the fit of each individual and drive the evolution of the QOC+GA. We employed a population ranging between 10 and 15 individuals for the first generation. The chromosomes of the individuals were randomly picked within specified intervals for each parameter; these intervals were proposed based on physical information or constraints of the system, the pulses and the target. For example, the field strength was limited to $E_0 \leq 3 \times 10^{10}$ V/m, similar to previous studies.[25] Different fitness functions were proposed for each of the different experiments of the present work; these will be described in detail in Sec. III. In general, fitness functions are designed to optimize the population that reaches a given target. The target could be a specific vibrational state, e.g., $\varphi_{X,0}$, or a more complex function involving several states. The optimal pulses were obtained by evolving the GA until the best value of the fitness function remained constant for at least 5 subsequent generations.

III. RESULTS AND DISCUSSION

We employed the methodology described in Sec. II with the aim of obtaining $\varphi_{X,0}$ molecules, starting from the initial states φ_{a,υ_a}, for υ_a = 20, 24, 29 in the $a^3\Sigma^+$ curve. For the assisted mechanism, we performed calculations for all three initial conditions υ_a = 20, 24, 29, and only results starting from an initial state $\varphi_{a,20}$ are presented for the direct mechanism. A comparison between initial states φ_{a,υ_a}, υ_a = 20, 24, 29, for the direct mechanism can be explored in a future work. For the assisted mechanism, we will only display results for $\varphi_{a,20}$, mentioning results for $\varphi_{a,24}$ and $\varphi_{a,29}$ only for comparison.

A. Time scales

It is important to consider the time scales associated with the vibrational dynamics on the PECs. In atomic units, the classical vibrational period of level υ can be estimated from[33] $T_{vib}(\upsilon) \approx 2\pi(\partial\upsilon/\partial E) \approx 4\pi|E_{\upsilon+1} - E_{\upsilon-1}|^{-1}$. The classical vibrational periods were calculated from our DVR eigenvalues for the electronic states $A^1\Sigma^+$, $X^1\Sigma^+$, and $b^3\Pi$. Resulting vibrational periods, $T_{vib}(\upsilon)$, range from 1.9×10^4 to 2.5×10^4 a.u., while the total time of the simulations for both direct and assisted mechanisms is at least 10 times longer than the typical $T_{vib}(\upsilon)$ of the pulse-coupled vibrational levels. The spin-orbit coupling between states $A^1\Sigma^+$ and $b^3\Pi$ is $\hat{W}_{bA} \approx 4 \times 10^{-4}$ a.u. We can estimate a typical time for the spin-orbit dynamics from Heisenberg uncertainty to obtain $\Delta t_{SOC} \approx 2.5 \times 10^3$ a.u., which is at least a hundred times smaller than the total simulation times employed in this work.

B. Direct mechanism

In the KRb [b-A]-scheme,[19] TMEs are large between high vibrational levels of the PECs, Fig. 2. The implementation of

TABLE I. Boundaries of the parameters of the LCPs belonging to the pump and dump frequency band.

Parameter	Minimum pump	Maximum pump pump	Minimum dump	Maximum dump
$E_0(10^{-3}$ a.u.)	5.0	10.0	5.0	10.0
$\tau_0(10^5$ a.u.)	1.1	1.5	2.1	3.5
$\tau(10^3$ a.u.)	2.0	80.0	2.0	80.0
$\omega(10^{-2}$ a.u.)	5.5	5.7	5.4	5.6

TABLE II. Optimized parameters of the LCPs belonging to the pump and dump pulses, when the fitness is set to the ground state.

Parameter	Optimal pump	Optimal dump
$E_0(10^{-3}$ a.u.)	5.08	9.16
$\tau_0(10^5$ a.u.)	2.02	3.79
$\tau(10^4$ a.u.)	6.48	2.06
$\omega(10^{-2}$ a.u.)	3.74	5.20

our QOC+GA method with a fitness function targeting only to the $X^1\Sigma^+$ state, regardless of the vibrational state v_X, results in vibrationally excited $X^1\Sigma^+$ molecules. In order to obtain $X^1\Sigma^+$ molecules directly in the ground vibrational state, we propose as fitness function

$$J_0 = \frac{\Pi_0}{1 - P_a}, \tag{8}$$

where

$$\Pi_0 = |\langle\varphi_{X,0}|\psi_X(t_{\max})\rangle|^2, \tag{9}$$

$$P_a = \langle\psi_a(t_{\max})|\psi_a(t_{\max})\rangle, \tag{10}$$

with $t_{\max}$ the final time of the simulation. In this fitness function, the denominator $1 - P_a$ stands for the population that left the state $a^3\Sigma^+$ at the final time. The fitness function, J_0, accounts for the fraction of $1 - P_a$ that reaches the target state $\varphi_{X,0}$ at time $t_{\max}$.

Genetic operations of the QOC+GA will generate genes and chromosomes within the ranges defined in Table I for the pump and dump pulses, respectively. The frequency boundaries of the pump pulse were chosen around the energy difference between the initial state, $\varphi_{a,20}$, and the vibrational levels of $b^3\Pi$ illustrated by the red circle of Fig. 2(a); for the dump pulse, the frequency boundaries were determined from the TMEs $\mu_{A,X}^{v_A,v_X=0}$ in a similar fashion [Fig. 2(c)]. It should also be pointed out that we studied only transform limited pulses, that is, $c = 0$. The evolution of the QOC+GA produced the optimal pulses described in Table II and Fig. 3(a), for the initial state $\varphi_{a,20}$.

Despite the significantly low TMEs involved in this stabilization scheme, the results are surprisingly satisfactory. The use of the fitness function in (8) in our QOC+GA scheme results in a population of 19.8% in the first 15 vibrational levels in $X^1\Sigma^+$, relative to the population leaving the initial state $\varphi_{a,20}$. Figure 3(b) displays the final distribution of the vibrational levels in $X^1\Sigma^+$. Although this is not a thermally stable distribution, it is important to notice that almost an 80% of the final $X^1\Sigma^+$ molecules are in levels $v_X < 15$. In absolute terms, the final population in the $X^1\Sigma^+$ state is less than the 1%. Besides to the fact of using low-intensity pulses, the pump process is considerably ineffective in this particular pathway; this is due to the small value of the TME coupling between the initial level $\varphi_{a,20}$ in $a^3\Sigma^+$ and the encircled vibrational levels in $b^3\Pi$ shown in Fig. 2(a).

The evolution of the electronic populations can be seen in Fig. 4. Panel (a) displays the effect of the pump pulse on the electronic populations, while panel (b) shows the combined effect of the SO coupling and the dump pulse on the populations of $b^3\Pi$, $A^1\Sigma^+$, and $X^1\Sigma^+$. It is noted the ineffectiveness of the pump process, barely 5% of the initial $\varphi_{a,20}$ is excited to the curve $b^3\Pi$. Panel (b) of Fig. 4 displays how effective are the SO coupling and the dump pulse populating the electronic curves $A^1\Sigma^+$ and $X^1\Sigma^+$. Table III summarizes the results for initial $\varphi_{a,20}$.

C. Assisted mechanism

The importance of the spin-orbit coupling (SOC) in the formation of deeply bound diatomic molecules using laser fields has been already investigated.[22,23] Ghosal and coworkers found that the magnitude of the spin-orbit coupling strongly affects the dynamics on the excited singlet and triplet electronic states of RbCs.[23] In the case of KRb, in Fig. 1(c), we can see that the SOC, W_{bA}, is approximately constant with lower value around the crossing between $b^3\Pi$ and $A^1\Sigma^+$. In the case of RbCs, it has been observed that for this "realistic" shape of the SOC, the dynamics on the excited curves are strongly nonadiabatic with important population transfer to the upper singlet curve. In the case of KRb, we expect to have a similar nonadiabatic dynamics on $A^1\Sigma^+$ and $b^3\Pi$, which could

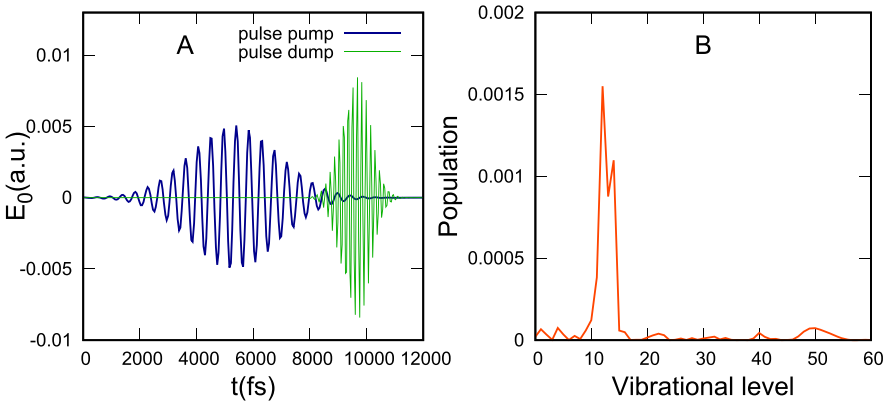

FIG. 3. (a) Time profile of pump (blue line) and dump (green line) pulses optimized to reach the final ground state. (b) Final composition of ground electronic state $X^1\Sigma^+$. Only the first 60 vibrational levels are included here.

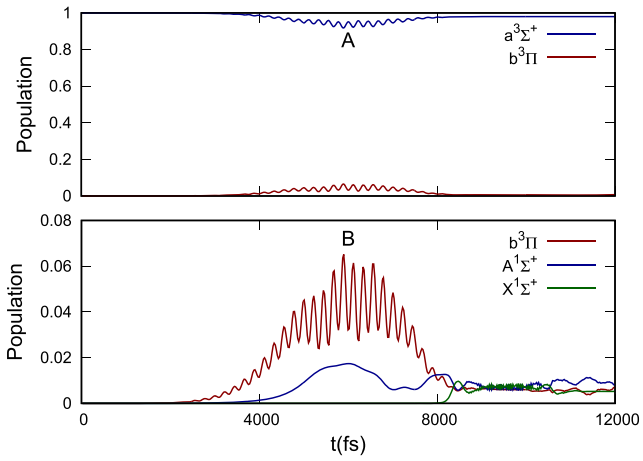

FIG. 4. Time- evolution of the populations belonging to (a) the singlet spin multiplicity $\{X^1\Sigma^+, A^1\Sigma^+\}$ and (b) the triplet spin multiplicity $\{a^3\Sigma^+, b^3\Pi\}$, using the fitness function in (8).

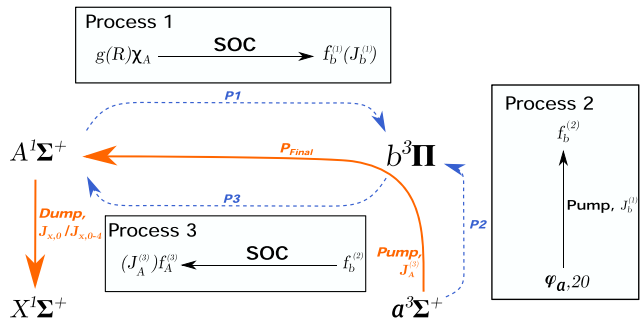

FIG. 5. Assisted mechanism. A systematic division of the complete vibrational stabilization process in three separable idealized stages: P1, P2, P3. The first stage produces an intermediate fitness function, $J_b^{(1)}$, used in the second stage. The second stage pumps the initial state $\varphi_{a,20}$, producing the wave packet $f_b^{(2)}$ in the electronic curve b. Stage 3 is a time evolution of $f_b^{(2)}$ on curves b and A under the effect of spin-orbit coupling to produce the effective fitness function $J_A^{(3)}$. In the pump stage, the initial wave function $\varphi_{a,20}$ is pumped to curves b and A using $J_A^{(3)}$ as fitness function. The dump stage uses two different fitness functions, $J_{X,0}$ and J_{0-4}, to optimize the dump pulse.

facilitate the transfer to deeply bound states of $X^1\Sigma^+$ by the use of a dump pulse.

An important conclusion of the works of Koch[22] and Ghosal[23] is that deeply bound singlet molecules could be formed based on an efficient mechanism for pump and dump steps. We propose an assisted mechanism that includes the effect of the SOC to obtain an optimal pump and dump pulses.

Defining the function $g(R) = \varphi_{X,0}(R)$, we identify $g(R)\chi_A$ as a wave function with the same shape of $\varphi_{X,0}(R)$ but on the electronic state $A^1\Sigma^+$. Figure 1 shows that the transition dipole moment d_{XA} is relatively constant for values of R around the minimum of the electronic curve $X^1\Sigma^+$; therefore, the wave function $g(R)\chi_A$ will have significant overlap with the target ground state $\varphi_{X,0}(R)$, being suitable to be efficiently transferred to the target state by the dump pulse. Figure 6(a) displays the vibrational composition of $g(R)\chi_A$, which has an approximate Gaussian shape centered at $\upsilon_A = 12$.

In this assisted approach, instead of setting a single fitness function, we use a systematic division of the complete stabilization process in three separable idealized stages, Fig. 5. For each of these stages, we find intermediate fitness functions obtained from identifying the vibrational composition on each PEC as a function of time. The outputs of these three stages are combined to obtain a fitness function for the QOC+GA scheme. The first idealized stage is a propagation of the initial condition $g(R)\chi_A$ on the electronic curves $A^1\Sigma^+$ and $b^3\Pi$; under the influence of the Hamiltonian in (7), the resulting wave packet is a transient vibrational distribution at time $t^{(1)}$ on curve $b^3\Pi$, $f_b^{(1)}$, which is used to build a fitness function for the second stage, $J_b^{(1)}$. The second stage optimizes a pulse shape capable of driving the system from the initial Feshbach state $\varphi_{a,20}$ to the target state $f_b^{(1)}$ using the QOC+GA scheme with the fitness function $J_b^{(1)}$ without SOC; this stage produces a final vibrational distribution, $f_b^{(2)}$, on curve $b^3\Pi$, which in turn is used as initial condition for the third stage. The third stage is a propagation, again with the (7) Hamiltonian that produces a transient vibrational distribution $f_A^{(3)}$ at time $t^{(3)}$ on curve $A^1\Sigma^+$; the distribution $f_A^{(3)}$ is used to build a target function $J_A^{(2)}$. Finally, we use QOC+GA with the fitness function $J_A^{(2)}$ to find an optimal pump pulse capable of driving the system from the initial wave function $\varphi_{a,20}$ to the target state $f_A^{(3)}$ in presence of the SOC. After the effect of the pump pulse, the system is on a nonstationary state that moves between curves $b^3\Pi$ and $A^1\Sigma^+$ by the effect of the SOC. We then use the QOC+GA method to find an optimal dump pulse with a well-defined fitness function targeting to the absolute ground vibrational state, $\varphi_{X,0}$.

TABLE III. Results from the first optimization approach, from $\varphi_{a,20}$, with a fitness aiming to a final ground state. Here, $\Pi_{X,\upsilon<15}$ accounts for the total population in the first 15 vibrational levels in $X^1\Sigma^+$.

Resulting yield (%)	Initial $\varphi_{a,20}$
Total $\Pi_{X,\upsilon<15}$	0.436
$\Pi_{X,\upsilon<15}$ as a fraction of $1 - P_a$	21.5
$\Pi_{X,\upsilon<15}$ as a fraction of $X^1\Sigma^+$	83.20

In the first stage, due to the SOC, $W_{bA}(R)$, the initial condition, $g(R)\chi_A$, evolves to a state delocalized between $b^3\Pi$ and $A^1\Sigma^+$, as can be seen in Fig. 7(a). It is shown in Fig. 7(a) that for time $t = 794.5$ fs, approximately half of the wave packet is located in curve $b^3\Pi$. The $b^3\Pi$-vibrational composition of the wave packet at $t = 794.5$ fs, $f_b^{(1)}$, can be seen in Fig. 6(b); it is worth to consider that this composition is centered at $\upsilon_b = 25$ and spread between $\upsilon_b = 20$ and $\upsilon_b = 30$. The vibrational composition $f_b^{(1)}$ can be used to design a fitness function to optimize the pump process. We propose a fitness function that is a linear combination of the five vibrational levels with the greatest contributions to the distribution in Fig. 6(b). This fitness function is given by

$$J_b^{(1)} = \frac{1}{P_{b^3\Pi}}\left[\Pi_{25} + \tfrac{1}{2}\Pi_{24} + \tfrac{1}{3}\Pi_{23} + \tfrac{1}{1.7}\Pi_{22} + \tfrac{2}{5}\Pi_{28}\right]. \quad (11)$$

The Π_υ are the vibrational populations on the curve $b^3\Pi$. The coefficients of the Π_υ are measured relative to the $\upsilon_b = 25$ level, with weight equal to 1. The denominator $P_{b^3\Pi}$ is the

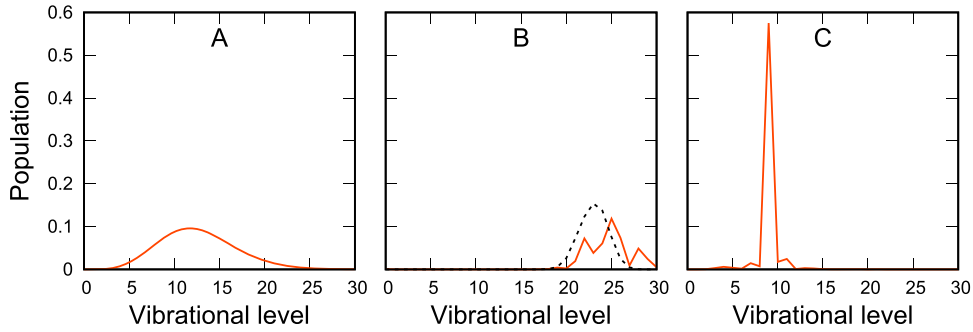

FIG. 6. (a) Vibrational composition of the wave function $g(R)\chi_A$. (b) Vibrational composition of the propagated wave function in the curve $b^3\Pi$, $f_b^{(1)}$, at time $t = 794.5$ fs. (c) Vibrational composition of $A^1\Sigma^+$ population maximum at $t = 597.1$ fs, after the pump scheme resulting population in $b^3\Pi$ is allowed to evolve via SOC, $f_A^{(3)}$. The vibrational distribution in state $b^3\Pi$ obtained with the pump pulse optimized by (11), $f_b^{(2)}$, is showed in dashed lines in (b).

population on curve $b^3\Pi$, which favors mainly the vibrational levels involved in the fitness function in (11).

The pump LCP is optimized by QOC+GA with the $J_b^{(1)}$ fitness function, fixing the central frequency of the laser ω to the energy difference between the levels $\upsilon_a = 20$ and $\upsilon_b = 25$; the time τ_0 is also fixed such that the pump pulse has a negligible effect at $t = 0$. The other parameters of the pump LCP are delimited within boundaries established in a similar manner as in Sec. III B, but now the pulse is slightly chirped positively. Pump pulse boundaries are listed in Table IV.

For the second stage, we used the $J_b^{(1)}$ fitness function [(11)], and a Hamiltonian that couples only the electronic curves $a^3\Sigma^+$ and $b^3\Pi$, to find an optimal pump pulse capable of producing the vibrational distribution $f_b^{(1)}$. It is worthy to remark that this pump process is not realistic because it does not include the SOC $W_{bA}(R)$, which acts permanently during the excitation process in the realistic scenario. This isolated pump process generates an initial condition located in curve $b^3\Pi$ only, $f_b^{(2)}$, which is shown in dashed lines in Fig. 6(b); we propagate this initial condition using the reduced Hamiltonian in (7). The electronic populations resulting from $f_b^{(2)}$ SOC evolution are shown in Fig. 7(b). A careful observation of this figure allows us to identify times at which the wave function is mostly located in $A^1\Sigma^+$. The vibrational distribution of curve $A^1\Sigma^+$ at $t = 597.1$ fs, $f_A^{(3)}$, can be seen in Fig. 6(c), which is narrowly centered at $\upsilon_A = 8$.

The previous results can be used to propose a new fitness function for the pump process, which accounts for both the pump and the SOC effects. This fitness function reads

$$J_A^{(1)} = \Pi_8, \tag{12}$$

with Π_8 as the population in the vibrational state $\varphi_{A,8}$.

TABLE IV. Boundaries of the parameters of the pump LCP in the assisted mechanism.

Parameter	Minimum	Maximum
$E_0(10^{-3}$ a.u.)	6.0	13
$\tau(10^3$ a.u.)	2.0	15
$c(10^{-9}$ a.u.)	1.0	100

For the final stage, we used QOC+GA with $J_A^{(1)}$ fitness function to find an optimal pump pulse capable of transferring the initial population from $a^3\Sigma^+$ to the vibrational state $\varphi_{A,8}$. After the pump pulse, the system evolves under the effect of the SOC. The electronic populations on curves $b^3\Pi$ and $A^1\Sigma^+$ are shown in Fig. 7(c) and show small oscillations around the value of 0.05, having some $A^1\Sigma^+$ electronic populations maximums for times $t > 4800$ fs. We look for a dump pulse with parameters within the ranges given in Table V. The frequency ω is

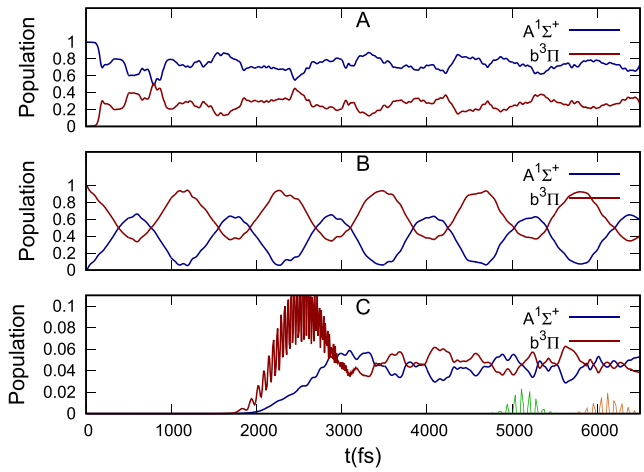

FIG. 7. (a) Time evolution of the electronic populations of $b^3\Pi$ and $A^1\Sigma^+$ due to the SOC, when $\varphi_{X,0}$ state is promoted to the curve $A^1\Sigma^+$; (b) $b^3\Pi$ and $A^1\Sigma^+$ SOC evolution after the initial pump pulse, and (c) the SOC evolution after the pump pulse is reoptimized. The positive section of the dump pulse representation in time for (13) (orange) and (14) (green) fitness functions is scaled and also showed in (c) for a better understanding of the dump scheme. Note that the population scale is different in (c).

TABLE V. Boundaries of the parameters of the LCPs belonging to the dump pulses for the assisted mechanism.

Parameter	Minimum	Maximum
$E_0(10^{-3}$ a.u.)	6.0	12
$\tau_0(10^5$ a.u.)	1.8	2.5
$\tau(10^3$ a.u.)	1.0	9.0
$\omega(10^{-2}$ a.u.)	5.1	5.3
$c(10^{-10}$ a.u.)	1.0	100

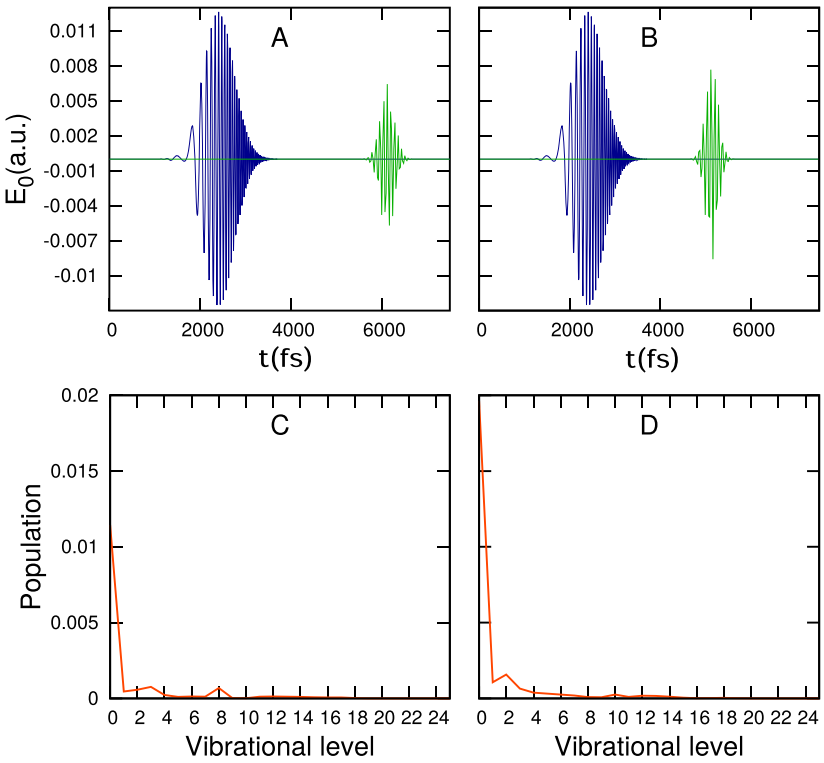

FIG. 8. (a) Pump (blue) and dump (green) pulses representation in time, for the fitness function in (13) and (b) for fitness in (14). (c) and (d) show the wave packet projection on the first 25 vibrational levels for the first and second fitness function, respectively.

narrowly set to the energy of the vibronic transition between the states $\varphi_{A,8}$ and $\varphi_{X,0}$.

To find an optimized dump pulse, two different fitness functions are proposed. The first fitness function targets only to the ground state $\varphi_{X,0}$,

$$J_0 = \Pi_0, \tag{13}$$

while the second fitness function targets to the first five vibrational levels in $X^1\Sigma^+$, seeking to obtain an overall vibrationally stable final state,

$$J_{0-4} = \sum_{i=0}^{4} \Pi_i. \tag{14}$$

The optimized pump and dump pulses, for J_0 and J_{0-4} fitness function, are shown in Figs. 8(a) and 8(b), respectively, and detailed in Table VI. For both fitness functions, the optimal pulses were capable of producing KRb molecules in the lower vibrational levels of the $X^1\Sigma^+$ curve, as can be seen in Figs. 8(c) and 8(b), respectively. Although the vibrational populations seem to be small, around 1%–2%, when these are measured relative to the amount transferred by the pump pulse, $1 - P_{a^3\Sigma^+}$, they become 12.6% and 21.5% for the first and second fitness functions, as can be seen in Table VII, respectively.

TABLE VI. Optimized parameters of the LCPs belonging to the pump and the dump frequency bands, where the values for the dump's two different fitness functions are listed separately.

Parameter	Optimal pump	Optimal dump (J_0)	Optimal dump (J_{0-4})
$E_0(10^{-3}$ a.u.)	12.6	6.55	8.70
$\tau_0(10^5$ a.u.)	1.00	2.54	2.13
$\tau(10^3$ a.u.)	14.1	6.49	5.63
$\omega(10^{-2}$ a.u.)	3.35	5.21	5.21
$c(10^{-9}$ a.u.)	65.4	9.95	6.95

Table VII also shows that for both fitness functions the absolute ground state $\varphi_{X,0}$ is nearly a 75% of the total population of the electronic state $X^1\Sigma^+$. Since the second fitness targets to the first 5 vibrational levels, it is interesting to observe the accumulated population of these levels as a fraction of $1 - P_{a^3\Sigma^+}$; Table VII displays these results. In this case, it is noticed that the second fitness function, (14), is more efficient achieving this target, leaving nearly half of the population in the excited electronic curves. Although the first fitness function was designed to target purely to the $\varphi_{X,0}$ state, it seems to be an unexpected result that the second fitness function is more efficient transferring to this state. The optimal values of the τ_0 for the pulses of Figs. 8(a) and 8(b) seem to be correlated with the times at which the $A^1\Sigma^+$ electronic population reaches a maximum. This is shown in the lower part of Fig. 7(c), where the pulses are indicated by the orange and green curves.

For the assisted mechanism, we compared the results of using $\varphi_{a,20}$ as initial state with those of using $\varphi_{a,24}$ and $\varphi_{a,29}$. The results from Table VII show that the stabilization yield for $\varphi_{a,20}$ is better than those of $\varphi_{a,24}$ and $\varphi_{a,29}$, which is due to the more favorable couplings of $\varphi_{a,20}$. Also, it is worth to mention that from an initial level $\upsilon_a = 29$, a greater fraction of the population excited by the pump pulse is transferred to the final state $\varphi_{X,0}$, than from the process with initial state $\varphi_{a,24}$, in spite of the fact that the TMEs $\mu_{a,b}^{\upsilon_a=29,\upsilon_b}$ is almost 2 orders of magnitude smaller than $\mu_{a=24,b}^{\upsilon_a,\upsilon_b}$. The aforementioned observation exemplifies the complexity of the vibrational stabilization mechanisms.

TABLE VII. Results from the second optimization approach. A and B refer to J_0 and J_{0-4} fitness functions.

Resulting yield (%)	$\varphi_{a,20}$ A	$\varphi_{a,20}$ B	$\varphi_{a,24}$ A	$\varphi_{a,24}$ B	$\varphi_{a,29}$ A	$\varphi_{a,29}$ B
Total yield at Π_0	1.14	1.96	0.0102	3.39×10^{-3}	0.0103	1.38×10^{-4}
Π_0 as fraction of $1-P_{a^3\Sigma^+}$	12.6	21.5	0.0467	0.0154	2.15	0.026
Π_0 as fraction of $P_{X^1\Sigma^+}$	75.1	77.9	0.237	0.0753	7.00	0.116
$\Pi_{0,4}$ as fraction of $1-P_{a^3\Sigma^+}$	14.8	25.6	0.101	4.19	14.0	11.13

IV. SUMMARY AND CONCLUSIONS

We have shown that a significant population transfer can be achieved from a weakly bound Feshbach resonance molecular state $\varphi_{a,20}$, to a singlet vibrational ground state $\varphi_{X,0}$, by the use of LCPs of duration in the order of picoseconds and that can easily be produced in a laboratory. As a result of a thorough analysis of the KRb system[19] and the aid of GAs,[43] after the effect of the pulses, we achieved an absolute 0.436% of transfer to the first 15 vibrational levels $\upsilon_X < 15$ of the $X^1\Sigma^+$ electronic state, when carrying out QOC calculations with a single fitness function and a basis set of Gaussian DC pulses. The same population transfer to levels $\upsilon_X < 15$, as a fraction of $1-P_{a^3\Sigma^+}$, turned out to be 5.91%. The direct vibrational stabilization scheme starting from higher excited Feshbach levels, such as $\upsilon_a = 24$ and 29, resulted in lower transfer yields due to less favorable FC coupling with the target state.

On the other hand, we proposed an optimization scheme in which we considered a sequence of three individual idealized processes. This separation resulted in an effective fitness function capable of producing an optimal pump pulse with the aid of a GA scheme. We proposed two different fitness functions for the dump process to produce vibrationally stable molecules in the $X^1\Sigma^+$ singlet. The implementation of the proposed vibrational stabilization scheme produced a transfer of 1.14% of the total population, when the dump pulse was optimized to reach the ground state $\varphi_{X,0}$ and 1.96% of the total population when it was optimized to reach the first five $X^1\Sigma^+$ levels, $\upsilon_X = 0$, 1, 2, 3, 4. When considered as fractions of the $1-P_{a^3\Sigma^+}$ population, these yields were 12.6% and 21.5%, respectively. The significant difference between the stabilization yields considered as fractions of the population transferred from $a^3\Sigma^+$ to $b^3\Pi$, and the absolute stabilization yield, establishes that the limiting step of the stabilization process is the pump transition, as most of the population remains on $a^3\Sigma^+$; this observation is explained by the fact that we are employing low-intensity laser pulses. It is also important to note that, as in the direct mechanism, the results obtained by setting level $\upsilon_a = 20$ as the initial state were more promising that those starting from $\upsilon_a = 24$ and 29, due to a more favorable TME coupling with the ground state.

The SO-assisted mechanism turned out to be significantly more efficient than the direct one. The transfer as a fraction of $1-P_{a^3\Sigma^+}$ was doubled using the SO-assisted mechanism, with the first dump fitness function, and it was almost 4 times greater with the second fitness function. These results showed that a thorough analysis of the stabilization process can undoubtedly improve the efficiency of the process. However, it must be pointed out that this analysis depends on particularities of each molecular system, contained in the TMEs.

Even though the overall yields obtained from our approaches are smaller than those obtained by other methods, the resulting pulses are simple enough to be reproduced with the current laser technology, in contrast with other methodologies that require a more complex configurations of the laser pulses.[4,19,25] Also, although our results present limitations, these can be improved by the use of gradient-based optimization methods supplementing the reported results and also using higher laser intensities constrained to the fulfillment of dipole and rotating wave approximations. Finally, the success of the proposed method for the KRb case shows great potential to be generalized and applied to other physical systems; we plan to address this directions in future works.

ACKNOWLEDGMENTS

This work was supported by Departamento Administrativo de Ciencia, Tecnología e Innovación, Colciencias, and Universidad Icesi. Colciencias financed this work through the Project No. 110665842793, "Formation and control of cold molecules," and Universidad Icesi co-founded this project under its internal research grants program. The authors thank Centro de Bioinformática y Biología Computacional de Colombia (BIOS) for allowing the use of their computational resources for our calculations.

[1] H. P. Büchler, E. Demler, M. Lukin, A. Micheli, N. Prokof'ev, G. Pupillo, and P. Zoller, Phys. Rev. Lett. **98**, 060404 (2007).
[2] A. Adams, L. D. Carr, T. Schäfer, P. Steinberg, and J. E. Thomas, New J. Phys. **14**(11), 115009 (2012).
[3] M. T. Bell and T. P. Softley, Mol. Phys. **107**(2), 99–132 (2009).
[4] K.-K. Ni, S. Ospelkaus, D. Wang, G. Quméner, B. Neyenhuis, M. H. G. de Miranda, J. L. Bohn, J. Ye, and D. S. Jin, Nature **464**, 1324–1328 (2010).
[5] G. Quéméner and P. S. Julienne, Chem. Rev. **112**(9), 4949–5011 (2012).
[6] D. DeMille, Phys. Rev. Lett. **88**, 067901 (2002).
[7] P. F. Weck and N. Balakrishnan, Int. Rev. Phys. Chem. **25**(3), 283–311 (2006).
[8] K.-K. Ni, S. Ospelkaus, M. H. G. De Miranda, A. Peér, B. Neyenhuis, J. J. Zirbel, S. Kotochigova, P. S. Julienne, D. S. Jin, and J. Ye, Science **322**(5899), 231 (2008).
[9] R. V. Krems, Phys. Chem. Chem. Phys. **10**, 4079–4092 (2008).
[10] C. A. Arango, M. Shapiro, and P. Brumer, Phys. Rev. Lett. **97**, 193202 (2006).
[11] R. V. Krems, Int. Rev. Phys. Chem. **24**(1), 99–118 (2005).
[12] H. L. Bethlem, G. Berden, and G. Meijer, Phys. Rev. Lett. **83**, 1558–1561 (1999).
[13] H. L. Bethlem and G. Meijer, Int. Rev. Phys. Chem. **22**(1), 73–128 (2003).
[14] N. Vanhaecke, U. Meier, M. Andrist, B. H. Meier, and F. Merkt. Phys. Rev. A **75**, 031402 (2007).
[15] E. Narevicius, C. G. Parthey, A. Libson, J. Narevicius, I. Chavez, U. Even, and M. G. Raizen, New J. Phys. **9**(10), 358 (2007).
[16] J. D. Weinstein, R. de Carvalho, T. Guillet, B. Friedrich, and J. M. Doyle, Nature **395**, 148–150 (1998).
[17] E. S. Shuman, J. F. Barry, and D. DeMille, Nature **467**, 820–823 (2010).
[18] K. Aikawa, D. Akamatsu, M. Hayashi, K. Oasa, J. Kobayashi, P. Naidon, T. Kishimoto, M. Ueda, and S. Inouye, Phys. Rev. Lett. **105**, 203001 (2010).

[19]D. Borsalino, B. Londoño-Floréz, R. Vexiau, O. Dulieu, N. Bouloufa-Maafa, and E. Luc-Koenig, Phys. Rev. A **90**(3), 033413 (2014).
[20]J. M. Sage, S. Sainis, T. Bergeman, and D. DeMille, Phys. Rev. Lett. **94**, 203001 (2005).
[21]K. V. Jones, E. Tiesinga, P. D. Lett, and P. S. Julienne, Rev. Mod. Phys. **78**, 483–535 (2006).
[22]C. P. Koch, R. Kosloff, and F. Masnou-Seeuws, Phys. Rev. A **73**, 043409 (2006).
[23]S. Ghosal, R. J. Doyle, C. P. Koch, and J. M. Hutson, New J. Phys. **11**, 055011 (2009).
[24]C. P. Koch and M. Shapiro, Chem. Rev. **112**(9), 4928 (2012).
[25]M. Ndong and C. P. Koch, Phys. Rev. A **82**, 043437 (2010).
[26]K. Bergmann, H. Theuer, and B. W. Shore, Rev. Mod. Phys. **70**, 1003–1025 (1998).
[27]N. V. Vitanov, M. Fleischhauer, B. W. Shore, and K. Bergmann, *Coherent Manipulation of Atoms Molecules by Sequential Laser Pulses*, Volume 46 of Advances in Atomic, Molecular, and Optical Physics (Academic Press, 2001), pp. 55–190.
[28]W. C. Stwalley, Eur. Phys. J. D **31**, 221–225 (2004).
[29]S. Ospelkaus, A. Pe'er, K.-K. Ni, J. J. Zirbel, B. Neyenhuis, S. Kotochigova, P. S. Julienne, J. Ye, and D. S. Jin, Nat. Phys. **4**, 622–626 (2008).
[30]S. T. Cundiff and J. Ye, Rev. Mod. Phys. **75**(1), 325–342 (2003).
[31]S. A. Malinovskaya and G. Liu, Chem. Phys. Lett. **664**, 1–4 (2016).
[32]J. Vala, O. Dulieu, F. Masnou-Seeuws, P. Pillet, and R. Kosloff, Phys. Rev. A **63**, 013412 (2000).
[33]E. Luc-Koenig, R. Kosloff, F. Masnou-Seeuws, and M. Vatasescu, Phys. Rev. A **70**, 033414 (2004).
[34]U. Poschinger, W. Salzmann, R. Wester, M. Weidemüller, C. P. Koch, and R. Kosloff, J. Phys. B: At., Mol. Opt. **39**(19), S1001 (2006).
[35]J. L. Carini, J. A. Pechkis, C. E. Rogers, P. L. Gould, S. Kallush, and R. Kosloff, Phys. Rev. A **87**, 011401 (2013).
[36]J. L. Carini, S. Kallush, R. Kosloff, and P. L. Gould, New J. Phys. **17**(2), 025008 (2015).
[37]J. L. Carini, S. Kallush, R. Kosloff, and P. L. Gould, Phys. Rev. Lett. **115**, 173003 (2015).
[38]J. L. Carini, S. Kallush, R. Kosloff, and P. L. Gould, J. Phys. Chem. A **120**(19), 3032–3041 (2016).
[39]A. Kaiser and V. May, Chem. Phys. **320**(2-3), 95–102 (2006).
[40]J. Werschnik and E. K. U. Gross, J. Phys. B: At., Mol. Opt. Phys. **40**, R175–R211 (2007).
[41]M. Ndong, H. Tal-Ezer, R. Kosloff, and C. P. Koch, J. Chem. Phys. **130**, 124108 (2009).
[42]C. P. Koch, J. P. Palao, R. Kosloff, and F. Masnou-Seeuws, Phys. Rev. A **70**, 013402 (2004).
[43]R. D. Guerrero, C. A. Arango, and A. Reyes, J. Chem. Phys. **143**(12), 124108 (2015).
[44]S. Kotochigova, P. S. Julienne, and E. Tiesinga, Phys. Rev. A **68**(2), 022501 (2003).
[45]J. Cao, C. J. Bardeen, and K. R. Wilson, Phys. Rev. Lett. **80**(7), 1406–1409 (1998).
[46]R. D. Guerrero, C. A. Arango, and A. Reyes, J. Chem. Phys. **145**(3), 031101 (2016).
[47]D. T. Colbert and W. H. Miller, J. Chem. Phys. **96**, 1982 (1992).